Soft Matter

PAPER

View Article Online
View Journal | View Issue

Cite this: *Soft Matter*, 2018, **14**, 7190

Effect of grafting density on conformation of poly(acrylic acid) in solution by dielectric spectroscopy†

Xinlu Zhou and Kongshuang Zhao *

Received 17th March 2018,
Accepted 2nd August 2018

DOI: 10.1039/c8sm00551f

rsc.li/soft-matter-journal

The effect of grafting density of poly(ethylene oxide) and dodecyl groups on the conformation of poly(acrylic acid) in solution was clarified by dielectric relaxation spectroscopy over a frequency range from 40 Hz to 110 MHz. Two distinct dielectric relaxations were found after the elimination of electrode polarization, and valuable information about the conformations and interfacial electrokinetic properties of molecules was obtained by analyzing the dielectric spectra based on a refined double-layer polarization model. The critical aggregation concentration was determined by the concentration dependency of dielectric parameters. The results based on zeta potential suggested that the ionization performance and behavior of counterion condensation were strongly influenced by the grafting density of poly(ethylene oxide) and dodecyl groups. The concentration dependency of correlation length, ratio of zeta potential, ratio of linear density of counterions, and the Debye length showed that the chain length and degree of intermolecular aggregation were also strongly influenced by the grafting density. We revealed the role of grafting density with respect to electrostatic interaction in determining the chain conformation of polyelectrolytes in solution.

1. Introduction

Polyelectrolytes containing hydrophilic/hydrophobic side chains offer a wide range of promising applications in drug delivery, cell encapsulation, and tissue engineering due to their structural diversities in solution. In these applications, chain conformation is controlled mainly through altering the composition, distribution, and density of side chains.[1–8] Fundamentally, the chain conformations of various polyelectrolytes in solution have been extensively investigated using molecular dynamics simulations and experimental measurements.[3,9–12] It has been reported that grafting density is one of the key elements in determining the microstructure and size of chains and intermolecular aggregations.[1,2,9–12]

Generally, grafting density affects the conformation by controlling the van der Waals interactions, *i.e.*, hydrogen bonding and hydrophobic interactions.[13,14] For example, by the dielectric spectroscopy method, Li *et al.*[13] found that poly(ethylene oxide) or dodecyl side chains enhanced the chain flexibility of poly(acrylic acid) by weakening the hydrogen bonding interactions between the carboxylic acid groups on the poly(acrylic acid) backbone. Furthermore, it is necessary to consider whether the grafting density can affect the conformation by controlling the Coulombic interactions between the charged monomers of polyelectrolytes.[15–19] Counterion condensation occurs when the thermal energy of the counterions is insufficient for them to escape the electric field generated by the effective charges on the chains.[20] Investigations into the above issues have become increasingly complex. So far, some studies have focused on the influence of grafting density on the effective charges on chains for polyelectrolytes with alkoxy or alkyl side chains.[15–19] However, these studies are fairly controversial. Some reports have demonstrated that increasing the grafting densities of alkoxy or alkyl side chains increases the effective charges on the chains,[15,16] but other studies have found that increasing the grafting densities decreases[17] or has no effect[18,19] on the effective charges on these chains. Additionally, these studies rarely consider the phenomenon of condensation of counterions. Therefore, the mechanism by which the grafting density affects the chain conformation needs to be further investigated.

Various experimental techniques have been used to investigate chain conformation or measure the effective charges on chains, and these techniques include light scattering, atomic force microscopy, viscosity measurement, potentiometric/conductance measurement, osmotic pressure measurement,[21–24] electron paramagnetic resonance (EPR), and anomalous small angle X-ray scattering (ASAXS).[25,26] Alternatively, dielectric relaxation

College of Chemistry, Beijing Normal University, Beijing 100875, China.
E-mail: zhaoks@bnu.edu.cn; Tel: +86-010-58805856

† Electronic supplementary information (ESI) available. See DOI: 10.1039/c8sm00551f

spectroscopy (DRS) has been widely used to study the structure and dynamics of polyelectrolytes in solution owing to its sensitivity to all kinds of polarizations. With appropriate dielectric models, DRS has been proved to yield valuable microlevel information about chain conformations, effective charges, distribution of counterions, *etc.*[27–34] For example, the double-layer polarization model (DLPM) was adopted to study the influence of chain conformation, counterion distribution, and net (electric) potential on dielectric relaxation.[33,34] Our previous study reported valuable information about chain conformation and electric charge characteristics of poly(acrylic acid) (PAA) or poly(acrylic acid) containing poly(ethylene oxide) (PEO)/dodecyl side chains in solution by analyzing DRS based on DLPM.[35,36] These studies have proved that dielectric spectroscopy is a promising tool to obtain additional microscale information about chain conformation and electric charge characteristics.

In the present study, we chose poly(acrylic acid)-*graft*-poly(ethylene oxide) (PAA-*g*-PEO) and poly(acrylic acid)-*graft*-dodecyl (PAA-*g*-dodecyl) with two different grafting densities in an aqueous solution, and their structures are described in Scheme 1. Dielectric measurements were carried out over a frequency range from 40 Hz to 110 MHz. Similar to that in our previous study,[35,36] some structural and electrical parameters were obtained by analyzing DRS based on DLPM. Based on the electrical parameters, we discussed the effect of grafting density on effective charges and the behavior of counterion condensation as well as the effect of grafting density on the degree of intermolecular aggregation. This finding will provide some insights into the potential mechanism by which the grafting density influences the chain conformation of polyelectrolytes.

2. DLP model

According to the double-layer polarization model (DLPM) of flexible polyelectrolytes in solution,[34] the dielectric response is closely related to the chain conformation and counterion distribution around the chain. In this model, polyelectrolyte chains with volume fraction φ are dispersed in a continuous medium with relative permittivity ε_s (Fig. 1a). A chain adopts a random walk configuration of correlation blobs with diameter ξ (termed as the correlation length) (Fig. 1b). A correlation blob is composed of several stiff subunits, which are assumed to be charged cylinders with radius a. The thickness of the electric double layer (EDL) around the charged cylinder is κ^{-1}. On the cylinder surface, $r \to a$, and electrical potential Ψ_0 is ζ, whereas far away from the cylinder, $r \to \infty$, and electrical potential Ψ is 0 (Fig. 1c).

When an ac electric current flows through the bulk and the double layer in series, two kinds of relaxation processes occur in the low-frequency (LF) range and high-frequency (HF) range. The HF relaxation is ascribed to the counterion fluctuation in the direction perpendicular to the chain axes, and the LF relaxation is due to the counterion fluctuation in the direction along the chain axes. The linear densities of the counterions that cause HF and LF relaxations are ρ_h and ρ_l, respectively. The complex permittivity $\varepsilon^*(\omega)$ is derived in the form of free energy storage and loss formula, which is a simple function of the parameters ξ, $\rho_{h,l}$, ζ, and κ^{-1} (please see eqn (S1)–(S9) in the ESI†).

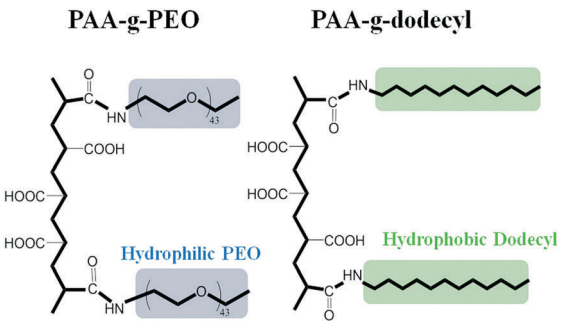

Scheme 1 Illustration of PAA-*g*-PEO and PAA-*g*-dodecyl molecules. The PEO and dodecyl side-chains are randomly distributed on the PAA main chain.

3. Experimental sections

3.1 Materials and preparation of the samples

PAA-*g*-PEO and PAA-*g*-dodecyl (Scheme 1) powders were prepared and purified by Prof. Charles C. Han's research group at the Institute of Chemistry, Chinese Academy of Sciences (Beijing, P. R. China). The method of preparing these polymers was described elsewhere.[14] According to the classical reaction of amino with carboxylic group, different contents of PEO ($M_w \approx$ 2000 g mol^{-1}) and dodecyl side chains were grafted onto the PAA ($M_w \approx$ 250 000 g mol^{-1}) main chains. The structures of these copolymers are presented in detail in Table 1.

A stock aqueous solution of PAA-*g*-PEO and PAA-*g*-dodecyl was prepared by initially dissolving 170 mg of PAA-*g*-PEO and PAA-*g*-dodecyl powders in 15 μL *N*,*N*-dimethyl formamide (DMF), followed by the addition of 10 ml double-distilled water (specific resistance was higher than 16 MΩ cm). The pH of the stock aqueous solution was adjusted to around 6.5 by the addition of KOH solution (0.5 mol L^{-1}). A series of aqueous solutions (0.025–2.5 mg ml^{-1}) were prepared by diluting a certain volume of the stock solution with double-distilled water.

3.2 Dielectric measurements

The dielectric measurements of PAA-*g*-PEO-7%, PAA-*g*-PEO-27%, PAA-*g*-dodecyl-10%, and PAA-*g*-dodecyl-34% aqueous solutions at different concentrations were carried out on a 4294A precision impedance analyzer (Agilent Technologies, USA) over a frequency range from 40 Hz to 110 MHz. A measuring cell with concentrically cylindrical platinum electrodes was employed to load the samples. The effective area of the electrodes was 78.5 mm^2, and the diameters of the inner and outer cylindrical electrodes were 5 mm and 10 mm, respectively. All the measurements were performed at about 30 ± 0.5 °C. The applied electric field strength in the dielectric measurements was 50–70 V m^{-1}. The measured raw data regarding capacitance C_x and conductance G_x were corrected to obtain the capacitance

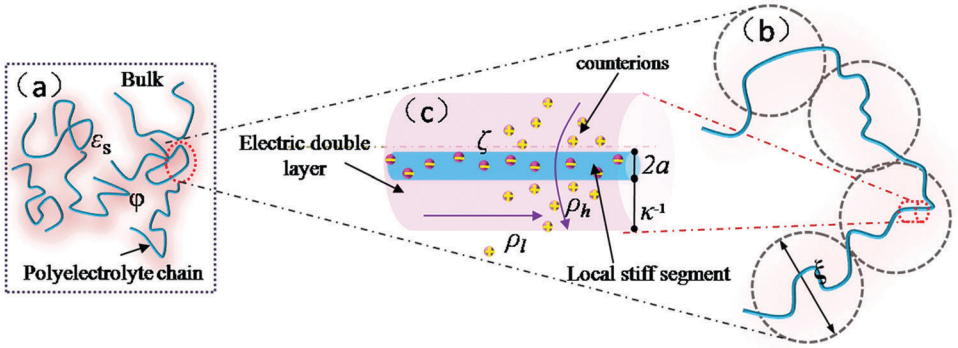

Fig. 1 Schematic diagram of the double-layer polarization model (DLPM) of flexible polyelectrolytes (PEs).[34] (a) PEs with occupied volume fraction φ are dispersed in a solvent with relative dielectric constant ε_s, (b) chain configuration of random walk of correlation blobs with volume ξ^3, and (c) local stiff segment with radius a and an electric double layer (EDL) with thickness κ^{-1}. Here, ζ is the surface potential of the local stiff segment, and ρ_l and ρ_h are the linear densities of the counterion fluctuations in directions along and perpendicular to the chain axes, respectively.

Table 1 Characteristics of PAA-*g*-PEO and PAA-*g*-dodecyl samples including molecular weight (M_w), molar fraction of side chains (f_{PEO}, $f_{dodecyl}$), and weight fraction of side chains (w_{PEO}, $w_{dodecyl}$)

	M_w/ 10^5	w_{PEO} (wt%)	$w_{dodecyl}$ (wt%)	f_{PEO} (mol%)	$f_{dodecyl}$ (mol%)
PAA-*g*-PEO-7%	2.75	7	—	0.27	—
PAA-*g*-PEO-27%	3.40	27	—	1.35	—
PAA-*g*-dodecyl-10%	2.80	—	10	—	4.2
PAA-*g*-dodecyl-34%	3.80	—	34	—	20

C_s and conductance G_s of the samples using the Schwan method;[37] then, they were converted to the corresponding permittivity ε' and conductivity κ using the equations $\varepsilon' = C_s/C_l$ and $\kappa = G_s\varepsilon_0/C_l$, respectively.

3.3 Dielectric analysis

Under an ac electric field, the dielectric response of a sample with angular frequency ω ($\omega = 2\pi f$, where f is the measurement frequency) was characterized by the complex permittivity $\varepsilon^*(\omega)$ as follows:

$$\varepsilon^*(\omega) = \varepsilon'(\omega) - j\varepsilon''(\omega) = \varepsilon(\omega) - j\frac{\kappa - \kappa_l}{\omega\varepsilon_0} \quad (1)$$

Here, $\varepsilon'(\omega)$ is the real part of the complex permittivity (also called permittivity), $\varepsilon''(\omega)$ is the imaginary part of the complex permittivity (also called dielectric loss), κ is the frequency-dependent conductivity, and κ_l is the low-frequency limit of conductivity. The dielectric loss data after eliminating the electrode polarization (EP) effect were obtained by subtracting κ_l through the equation $\varepsilon''(\omega) = (\kappa(\omega) - \kappa_l)/\varepsilon_0\omega$. The dielectric loss spectra were well fitted by the Cole–Cole function after eliminating the EP effect (Fig. 2), and the representative dielectric loss spectra of the sample at varying concentrations are shown in the inset of Fig. 2. Remarkably, two distinct peaks were found in the dielectric loss spectra (Fig. 3a and b).

The DLP model of flexible polyelectrolytes[34] was adopted to analyze two relaxations found in this study. By combining eqn (S1)–(S4) and (S6)–(S8) (ESI†), the dielectric function $\varepsilon^*(\omega)$ in the framework of the DLP theory including two relaxation terms and electrode polarization term was obtained. Then, the real part of the dielectric function $\varepsilon'(\omega)$ was employed to fit the experimental permittivity spectrum with electrode polarization (EP) effect. The best curve-fitting was guaranteed by the nonlinear least-squares method. Fig. 3 shows one of the fitting results of experimental permittivity spectra after eliminating the EP effect for PAA-*g*-PEO-27% and PAA-*g*-dodecyl-34% aqueous solutions with DLPM. This result showed that the DLP theory is fairly accurate in fitting the experimental permittivity spectra. Thus, according to the DLP theory, the LF and HF relaxations (clearly presented in Fig. 2) originate from the counterion fluctuations in the directions along and perpendicular to the PE chain axes, respectively. By means of fitting, many valuable structural and electrical parameters (ξ, ρ_l, ρ_h, and κ^{-1}) of the four samples were obtained. Meanwhile, LF and HF relaxation increments ($\Delta\varepsilon_l$ and $\Delta\varepsilon_h$) were calculated by substituting ρ_l, ρ_h, κ^{-1}, and ξ into eqn (S3), (S4) and (S7), (S8) (ESI†), respectively. Then, the ζ potential of the local stiff segments was calculated by substituting the parameters ρ_l, ρ_h, and κ^{-1} into eqn (S5) and (S9) (ESI†). The obtained parameters are listed in Table 2.

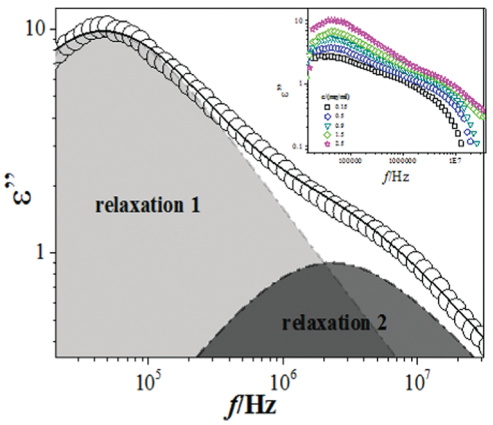

Fig. 2 The representative dielectric loss spectra fitted with the Cole–Cole function for PAA-*g*-PEO-7% solution at 2.5 mg ml^{-1}, and the inset is the dielectric loss spectra for PAA-*g*-PEO-7% solutions at varying concentrations.

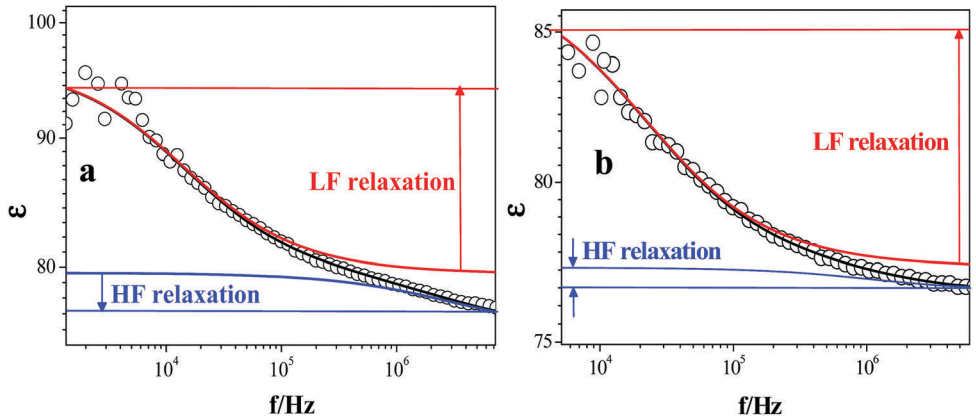

Fig. 3 The representative permittivity spectra of PAA-*g*-PEO-27% (a) and PAA-*g*-dodecyl-34% (b) solutions at 0.1 mg ml^{-1} fitted with DLPM using the following parameters: Bjerrum length l_B = 0.714 nm, diffusivity of potassium ions $D = 0.74 \times 10^8$ nm^2 s^{-1},[38] and measured solvent viscosity $\eta \approx 0.8 \times 10^{-3}$ N s m^{-2}. Hollow circles represent the experimental permittivity data, and solid lines represent the theoretical permittivity data calculated by DLPM. The low-frequency (LF) and high-frequency (HF) relaxations are represented by solid red and blue lines, respectively.

4. Results and discussion

4.1 Concentration dependency of dielectric spectra

4.1.1 PAA-*g*-PEO molecules in aqueous solution. The permittivity spectra of PAA-*g*-PEO-7% and PAA-*g*-PEO-27% at different concentrations are shown in Fig. 4. At first, it can be seen that the permittivity decreased sharply as the frequency increased below approximately 10^5 Hz, which has been widely recognized as the so-called electrode polarization effect. The ion strength in the polyelectrolyte solution was larger, and the electrode polarization (EP) contribution at a lower frequency was clear and may cover the LF relaxation.[39] With the increasing concentration of the samples, the concentration of counterions (q_c) increased, leading to higher electrode polarization. Theoretically, the concentration of the counterions (q_c) is inversely proportional to the Debye screening length (κ^{-1}) in a solution of polyelectrolytes without the addition of salt.[40]

$$\kappa^2 = 4\pi l_B z_c {q_c}^2 \quad (2)$$

Here, z_c is the valence of counterions. Experimentally, we have obtained the result for κ^{-1} of the four systems at different concentrations using dielectric analysis based on the DLP model. As shown in Fig. 12a and b, κ^{-1} decreased with increasing concentrations. According to eqn (2), q_c increased with increasing concentrations. Therefore, electrode polarization increased with an increase in concentration, leading to an increase in the decreasing rate of permittivity (Fig. 4).

To determine the concentration dependency of the dielectric spectra of PAA-*g*-PEO solution, the permittivity (ε_0) at a higher frequency of 1×10^6 Hz (Fig. 4) was plotted against concentration. As shown in the insets of Fig. 4, inflections occurred around 0.2 mg ml^{-1} and 0.4 mg ml^{-1} for PAA-*g*-PEO-7% and PAA-*g*-PEO-27% solutions, respectively. Similar transition concentrations were also found in the concentration dependency of dielectric increment and relaxation times of LF and HF (Fig. 5). According to the previous study of our research group,[41] molecules evenly and separately disperse in an aqueous solution at low concentrations. When the concentration reaches around 0.2 mg ml^{-1}, molecules begin to aggregate because of the intermolecular interactions of the H-bond associations. The transition concentrations were also represented as the critical aggregation concentration c_p^r. According our study, the orders of magnitudes of the transition concentrations of PAA-*g*-PEO-7% and PAA-*g*-PEO-27% solutions (insets of Fig. 4 and 5) were in agreement with the above results. This suggested that the transition concentration is the critical aggregation concentration c_p^r.

From the insets of Fig. 4, below c_p^r, the permittivity around 1×10^6 Hz increased with the increasing concentrations; above c_p^r, this trend became slower. The polarization of the systems around 1×10^6 Hz is divided into two parts: counterion fluctuations perpendicular to the chain axis, which are caused by the HF fluctuations, as mentioned in Section 3.3, and the solvent. The contribution of counterion fluctuations perpendicular to the chain axis to the permittivity around 1×10^6 Hz could be estimated by the result of $\Delta\varepsilon_h$ (Fig. 5d). The results showed that the dielectric increment ($\Delta\varepsilon_h$) caused by the counterion fluctuations perpendicular to the chain axis increased as the concentrations increased below c_p^r, and it decreased above c_p^r. This may explain the slower increase in permittivity with concentration above c_p^r. In general, for a polyelectrolyte solution, $\Delta\varepsilon_h$ is proportional to the concentration of counterions (q_c) and the fluctuation distance, namely, the correlation length ξ, according to the equation $\Delta\varepsilon_h \sim q_c\xi$.[32] For PAA-*g*-PEO in our study, above c_p^r, with increasing concentrations, intermolecular hydrogen bonds could be formed between the alkoxy groups of the PEO side chains and carboxyl groups of the PAA main chain,[14] which inhibited the dissociation of carboxyl groups to a certain extent. Therefore, the increase in q_c was not clear above c_p^r. This conjecture is confirmed by the concentration dependency of κ^{-1} obtained by the dielectric analysis of the DLP model, as described in Section 3.3. As shown in Fig. 12a, the decrease in κ^{-1} with concentration above c_p^r was slower than that below c_p^r. According to eqn (2), we know that the increase in q_c above c_p^r is

Table 2 Structural and electrical parameters of PAA-*g*-PEO and PAA-*g*-dodecyl molecules

PAA-*g*-PEO-7%							
c (mg ml^{-1})	$10^{19}\rho$ (C nm^{-1})	ξ (nm)	ζ (mV)	$\Delta\varepsilon_l$	$\Delta\varepsilon_h$	τ_l (μs)	τ_h (ns)
2.5	6.43 ± 0.02	18.51 ± 0.22	2.41 ± 0.06	21.21 ± 0.12	1.42 ± 0.05	7.51 ± 0.18	63.71 ± 0.82
1.5	6.01 ± 0.02	20.82 ± 0.20	3.32 ± 0.08	19.12 ± 0.09	1.25 ± 0.07	8.91 ± 0.15	77.64 ± 0.96
0.9	6.27 ± 0.01	24.36 ± 0.34	3.89 ± 0.08	14.51 ± 0.13	1.31 ± 0.09	9.50 ± 0.13	77.60 ± 0.92
0.5	6.22 ± 0.02	28.83 ± 0.15	5.03 ± 0.09	11.83 ± 0.12	1.54 ± 0.06	11.92 ± 0.17	117.56 ± 1.52
0.25	4.72 ± 0.01	35.02 ± 0.17	8.54 ± 0.07	12.20 ± 0.15	2.61 ± 0.03	16.73 ± 0.17	252.24 ± 1.78
0.15	5.21 ± 0.02	36.01 ± 0.19	14.21 ± 0.07	11.43 ± 0.11	2.84 ± 0.05	20.02 ± 0.15	353.73 ± 1.93
0.1	5.00 ± 0.03	37.51 ± 0.23	21.32 ± 0.11	10.92 ± 0.10	2.10 ± 0.02	17.52 ± 0.16	353.73 ± 1.98
0.05	5.42 ± 0.03	42.02 ± 0.26	35.41 ± 0.12	10.61 ± 0.15	1.40 ± 0.03	20.01 ± 0.18	378.92 ± 2.05
0.025	5.88 ± 0.04	47.02 ± 0.29	53.13 ± 0.11	9.32 ± 0.11	1.80 ± 0.03	36.73 ± 0.19	720.70 ± 3.75
PAA-*g*-PEO-27%							
c (mg ml^{-1})	$10^{19}\rho$ (C nm^{-1})	ξ (nm)	ζ (mV)	$\Delta\varepsilon_l$	$\Delta\varepsilon_h$	τ_l (μs)	τ_h (ns)
2.5	15.42 ± 0.05	19.51 ± 0.26	7.42 ± 0.21	51.80 ± 0.19	1.12 ± 0.05	25.02 ± 0.25	53.00 ± 0.72
1.5	15.31 ± 0.04	22.52 ± 0.29	8.30 ± 0.22	41.70 ± 0.17	2.72 ± 0.05	30.31 ± 0.23	83.83 ± 0.85
0.9	15.44 ± 0.05	25.50 ± 0.22	10.00 ± 0.19	28.62 ± 0.15	2.51 ± 0.07	42.61 ± 0.28	199.53 ± 1.82
0.5	15.31 ± 0.07	32.00 ± 0.23	12.37 ± 0.15	26.51 ± 0.21	3.73 ± 0.08	54.45 ± 0.30	332.62 ± 2.76
0.25	14.34 ± 0.08	33.02 ± 0.23	21.03 ± 0.11	23.20 ± 0.22	3.81 ± 0.06	56.64 ± 0.32	381.71 ± 2.52
0.15	14.30 ± 0.05	35.51 ± 0.27	25.92 ± 0.12	17.00 ± 0.12	3.10 ± 0.05	57.61 ± 0.35	397.92 ± 3.52
0.1	14.29 ± 0.05	37.04 ± 0.35	33.71 ± 0.22	14.50 ± 0.15	2.84 ± 0.03	58.30 ± 0.32	454.72 ± 3.92
0.05	14.25 ± 0.08	39.01 ± 0.32	61.21 ± 0.29	13.92 ± 0.12	1.94 ± 0.02	59.62 ± 0.30	558.44 ± 4.22
0.025	14.28 ± 0.05	40.01 ± 0.21	84.14 ± 0.28	9.81 ± 0.16	1.22 ± 0.02	60.60 ± 0.28	636.63 ± 4.84
PAA-*g*-dodecyl-10%							
c (mg ml^{-1})	$10^{19}\rho$ (C nm^{-1})	ξ (nm)	ζ (mV)	$\Delta\varepsilon_l$	$\Delta\varepsilon_h$	τ_l (μs)	τ_h (ns)
2.5	8.50 ± 0.04	29.02 ± 0.15	9.19 ± 0.21	15.82 ± 0.08	2.22 ± 0.04	21.90 ± 0.21	106.12 ± 1.68
1.5	7.82 ± 0.03	30.02 ± 0.19	10.72 ± 0.24	12.11 ± 0.09	2.01 ± 0.07	23.62 ± 0.22	106.14 ± 1.73
0.9	7.21 ± 0.05	32.01 ± 0.19	10.64 ± 0.21	11.42 ± 0.07	1.61 ± 0.08	25.44 ± 0.21	106.14 ± 1.79
0.5	6.61 ± 0.07	33.05 ± 0.12	9.22 ± 0.25	6.74 ± 0.05	0.83 ± 0.03	27.62 ± 0.24	106.13 ± 1.63
0.25	6.39 ± 0.05	35.32 ± 0.23	19.76 ± 0.28	6.82 ± 0.05	0.81 ± 0.04	29.13 ± 0.28	106.10 ± 1.76
0.15	6.22 ± 0.05	36.53 ± 0.26	24.55 ± 0.29	5.33 ± 0.04	0.63 ± 0.02	34.78 ± 0.29	122.42 ± 1.79
0.1	6.01 ± 0.05	37.04 ± 0.27	32.88 ± 0.27	4.76 ± 0.03	0.52 ± 0.05	36.80 ± 0.21	132.62 ± 1.82
0.05	5.61 ± 0.05	38.03 ± 0.24	50.71 ± 0.25	3.72 ± 0.06	0.41 ± 0.08	38.32 ± 0.22	151.61 ± 1.85
0.025	5.14 ± 0.09	39.52 ± 0.22	56.81 ± 0.21	3.51 ± 0.05	0.20 ± 0.05	40.01 ± 0.22	187.23 ± 1.72
PAA-*g*-dodecyl-34%							
c (mg ml^{-1})	$10^{19}\rho$ (C nm^{-1})	ξ (nm)	ζ (mV)	$\Delta\varepsilon_l$	$\Delta\varepsilon_h$	τ_l (μs)	τ_h (ns)
2.5	9.60 ± 0.06	28.02 ± 0.13	17.58 ± 0.26	23.90 ± 0.11	4.00 ± 0.03	34.01 ± 0.27	95.95 ± 1.64
1.5	9.45 ± 0.05	29.01 ± 0.14	24.17 ± 0.28	16.12 ± 0.10	3.12 ± 0.03	35.13 ± 0.25	95.95 ± 1.53
0.9	9.43 ± 0.09	29.51 ± 0.12	31.56 ± 0.25	11.62 ± 0.10	2.42 ± 0.02	37.91 ± 0.25	95.95 ± 1.51
0.5	9.32 ± 0.04	31.53 ± 0.14	33.26 ± 0.24	9.11 ± 0.12	1.44 ± 0.01	39.54 ± 0.24	95.95 ± 1.51
0.25	9.32 ± 0.05	33.04 ± 0.12	32.29 ± 0.29	7.14 ± 0.14	0.84 ± 0.07	42.73 ± 0.28	95.95 ± 1.62
0.15	9.10 ± 0.05	35.52 ± 0.14	34.83 ± 0.31	6.47 ± 0.08	0.62 ± 0.03	48.52 ± 0.22	126.43 ± 1.63
0.1	7.63 ± 0.05	36.51 ± 0.15	32.18 ± 0.25	6.10 ± 0.09	0.51 ± 0.02	57.03 ± 0.25	171.53 ± 1.65
0.05	7.54 ± 0.07	37.5 ± 0.19	34.45 ± 0.27	4.73 ± 0.08	0.31 ± 0.03	59.02 ± 0.23	171.53 ± 1.72
0.025	7.53 ± 0.06	38.5 ± 0.19	38.85 ± 0.26	3.72 ± 0.08	0.20 ± 0.05	62.53 ± 0.23	180.84 ± 1.70

slower than that below c_p^r. In addition, the concentration dependency of ξ was also obtained (Fig. 10). We know that ξ decreases with an increase in concentration. Therefore, according to the equation $\Delta\varepsilon_h \sim q_c\xi$, above c_p^r, $\Delta\varepsilon_h$ decreased, and the permittivity around 1×10^6 Hz increased more slowly with the increasing concentration.

In addition, according to the counterion fluctuation theory,[32] the diffusion distance of the counterions that is perpendicular to the chain axes is proportional to the distance between the chains, and the scaling relation between the dielectric increment and the concentration below c_p^r is given by $\Delta\varepsilon_h \sim c^{1/3}$. According to the Zimm model,[42] the distance that the counterions diffuse perpendicular to the chain axes is proportional to the hydrodynamic volume of the chain, and the scaling relationship between the dielectric increment and concentration is given by $\Delta\varepsilon_h \sim c^{3/5}$. From Fig. 5d, it is evident that the scaling relationship for PAA-*g*-PEO-7% can be expressed as $\Delta\varepsilon_h \sim c^{0.63}$, which is close to $\Delta\varepsilon_h \sim c^{3/5}$ described by the Zimm model; moreover, the scaling relationship for PAA-*g*-PEO-27% is given by $\Delta\varepsilon_h \sim c^{0.36}$, which is close to $\Delta\varepsilon_h \sim c^{1/3}$ described by the Ito model.

4.1.2 PAA-*g*-dodecyl molecules in aqueous solutions. The permittivity spectra of PAA-*g*-dodecyl-10% and PAA-*g*-dodecyl-34% at different concentrations are shown in Fig. 6. The values of permittivity at 1×10^6 Hz against concentration are plotted in the insets of Fig. 6. Similarly, the inflection points were

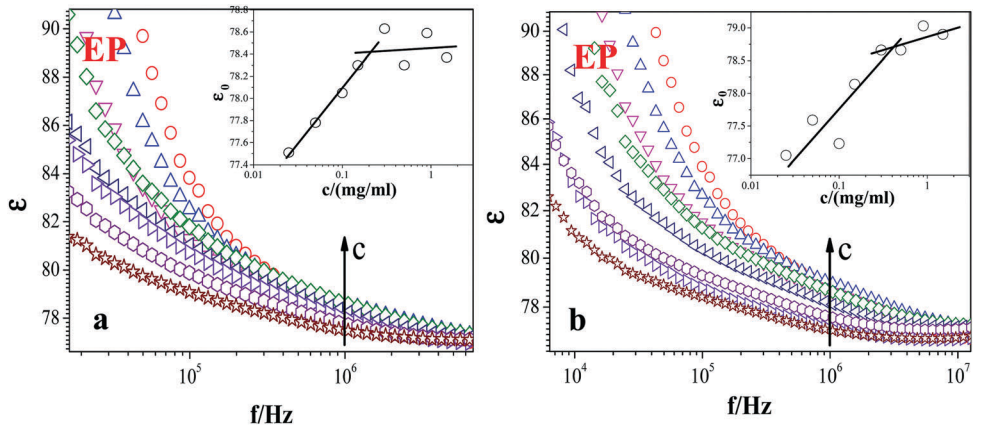

Fig. 4 Dielectric spectra of PAA-*g*-PEO-7% (a) and PAA-*g*-PEO-27% (b) at different concentrations. EP: electrode polarization at low frequencies. The insets show the concentration dependence of permittivity at a fixed frequency of 1×10^6 Hz.

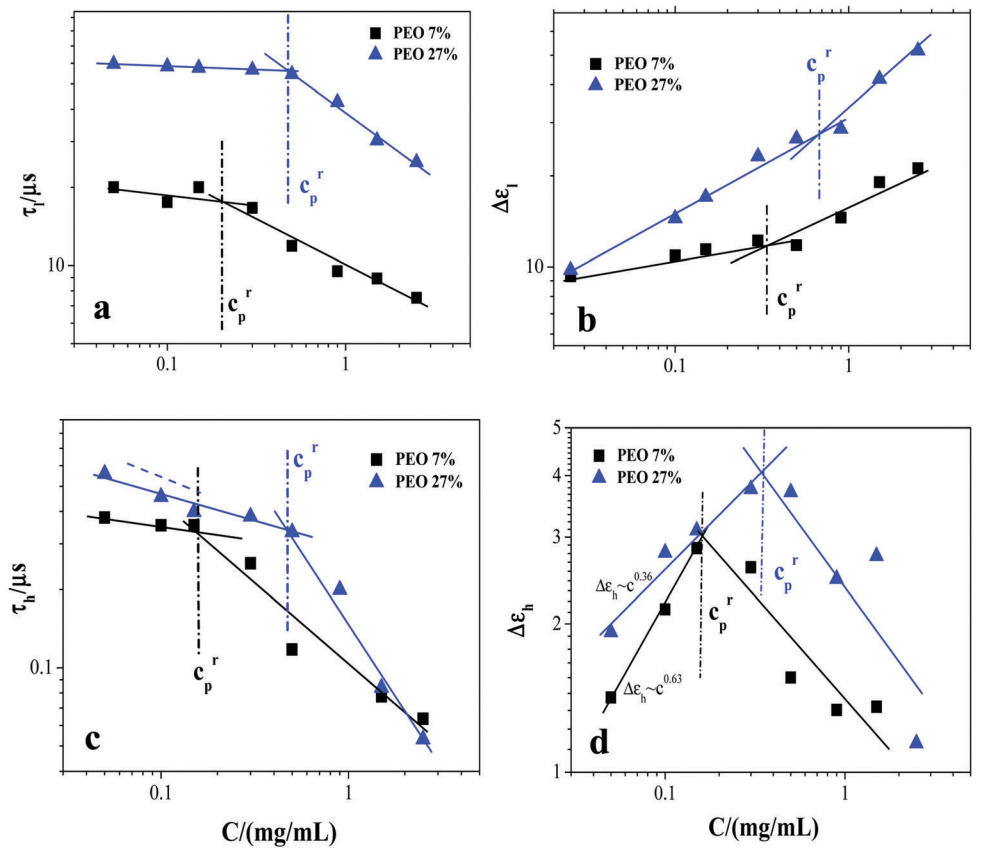

Fig. 5 Concentration dependency of LF and HF relaxation times (a and c) and dielectric increments (b and d) for PAA-*g*-PEO-7% and PAA-*g*-PEO-27% in an aqueous solution.

found at around 0.3 mg ml^{-1} and 0.1 mg ml^{-1} for PAA-*g*-dodecyl-10% and PAA-*g*-dodecyl-34%, respectively. Furthermore, the inflection points were close to those found in the concentration dependence of the dielectric parameters in Fig. 7. It has been widely accepted that PAA-*g*-dodecyl molecules exist in the form of a single chain in solution in dilute concentration range. When the concentration is raised to a certain value, intermolecular aggregates are formed.[43–45] When the concentration continues to rise to a certain higher value, aggregated chains start to overlap; such overlapping chains exist in the form of gelatin, and the non-overlapping chains exist in the form of sol.[46] According to the study reported by Hao *et al.*, aggregation is observed around 0.27 mg ml^{-1},[14] which was close to the inflection concentration as shown in the insets of Fig. 6 and 7. Therefore, it could be concluded that the inflection concentration is also critical aggregation concentration (c_p^r).

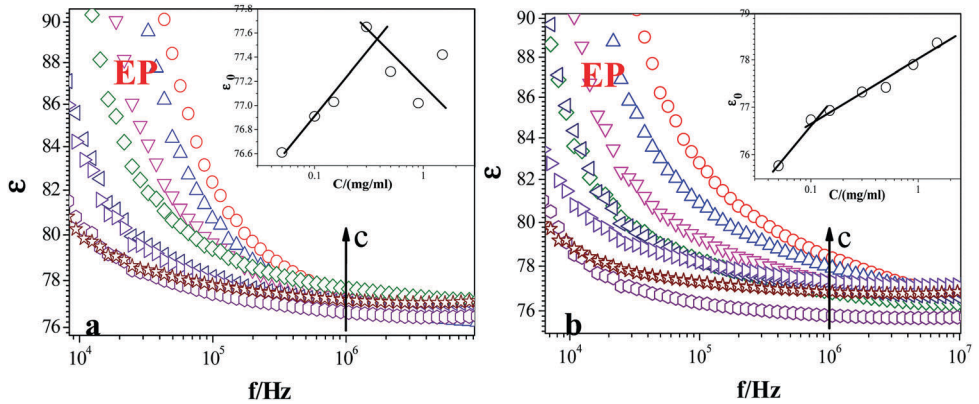

Fig. 6 The permittivity spectra of PAA-*g*-dodecyl-10% (a) and PAA-*g*-dodecyl-34% (b) at different concentrations. EP: electrode polarization at low frequencies. The insets show the concentration dependence of permittivity at a fixed frequency of 1×10^6 Hz.

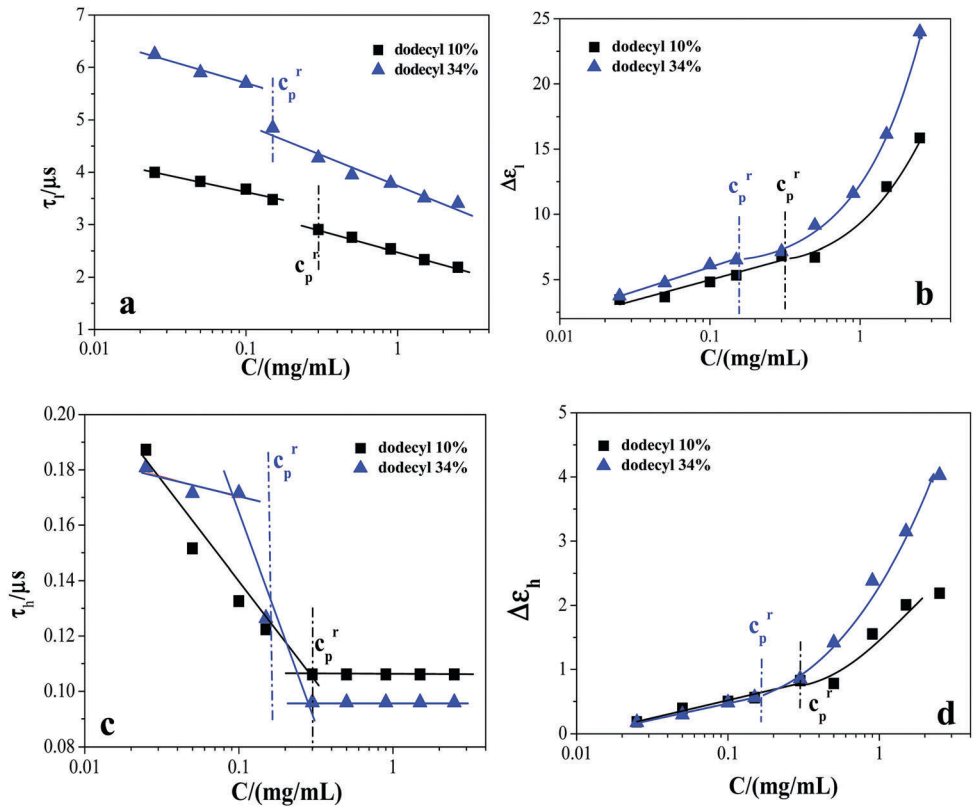

Fig. 7 Concentration dependency of LF and HF relaxation times (a and c) and dielectric increments (b and d) for PAA-*g*-dodecyl-10% and PAA-*g*-PEO-34% (a and b) in an aqueous solution.

In addition, as seen in the insets of Fig. 6a and b, below c_p^r, the permittivities of PAA-*g*-dodecyl-10% and PAA-*g*-dodecyl-34% solutions increase with the increasing concentrations; above c_p^r, the permittivity of the PAA-*g*-dodecyl-34% solution decreases and that of the PAA-*g*-dodecyl-10% solution increases more slowly. Similar to that for the PAA-*g*-PEO solution, at around 10^6 Hz, the polarization of the PAA-*g*-dodecyl aqueous solutions originates from both the counterion fluctuations perpendicular to the chain axis and water molecules. As shown in Fig. 7d, dielectric increment ($\Delta\varepsilon_h$) caused by the counterion fluctuations perpendicular to the chain axis increases with the increasing concentration more quickly. This indicates that the trend in which the permittivity at 10^6 Hz decreases or increases more slowly above c_p^r (inset of Fig. 6) may be due to water molecules. It can be expected that above c_p^r, intermolecular hydrophobic microdomains form continuously; this might lead to the growth of the hydrated shell of hydrophobic microdomains, which gradually decreases the polarization of the water molecules upon the increase in concentration.[47]

4.2 The role of grafting density in electric charge characteristics

4.2.1 PAA-*g*-PEO molecules in aqueous solutions. The effective charges on chains can be reflected by the ζ potential on the local stiff segments. The ζ potentials (Table 2) were plotted as a function of the concentrations of PAA-*g*-PEO-7% and PAA-*g*-PEO-27% (Fig. 8). It was found that the ζ potentials of PAA-*g*-PEO-27% were larger than those of PAA-*g*-PEO-7%, suggesting that the effective charges on the PAA-*g*-PEO-27% molecules are more. In other words, an increase in the grafting density of the PEO groups increased the effective charges on the PAA molecules. This result can be due to two aspects: (1) the steric hindrance effect of the PEO side chains described by K. Benmansour *et al.* due to which less space is available to accommodate condensed counterions[17,35] and (2) the gradual breaking of H-bonds between the carboxyl groups of the PAA main chains and the alkoxy groups of the PEO side chains as the concentration decreases,[14] leading to further dissociation of the carboxyl groups. It is reasonably expected that the PAA-*g*-PEO molecules containing more PEO side chains have stronger steric hindrance effect and dissociate more hydrogen ions in the process of solution dilution. Therefore, the effective charges on the PAA-*g*-PEO-27% molecules are more than those on the PAA-*g*-PEO-27% molecules over the entire concentration range.

Moreover, Fig. 8 shows that the ζ potentials of both PAA-*g*-PEO-27% and PAA-*g*-PEO-7% in an aqueous solution decrease logarithmically with increasing concentration. This suggests that the trend of counterion condensation with increasing concentration is less influenced by the grafting density of the PEO side chains. According to the Manning's counterion condensation theory,[48,49] the fraction of effective charges on the polyelectrolyte chains decreases logarithmically with increasing concentration in a good or theta solvent when the fraction of the effective charges on the chain in an extremely dilute solution increases beyond a critical value of f_c ($\approx b/l_B$, where l_B is the Bjerrum length and b is the bond size). In this study, the values for the fraction of the effective charges of PAA-*g*-PEO-7% and PAA-*g*-PEO-27% at the lowest concentration of 0.025 mg ml^{-1} are estimated by the results of linear density of counterions (ρ) (Table 2), and these values are close to 0.89 and 1, respectively. This result meets the critical condition of Manning condensation. Therefore, we observe the trend of logarithmical decrease of ζ potentials (Fig. 8). Thus, the PAA-*g*-PEO molecules in solution exhibit Manning-like counterion condensation.

4.2.2 PAA-*g*-dodecyl molecules in aqueous solutions. The concentration dependency of the ζ potential of PAA-*g*-dodecyl-10% and PAA-*g*-dodecyl-34% molecules in an aqueous solution is shown in Fig. 9. There are remarkable differences between the results regardless of the value or trend. This result proves that the behavior of the counterion condensation of PAA-*g*-dodecyl molecules is affected by the grafting density. For PAA-*g*-dodecyl-10%, it is evident from Fig. 9 that the ζ potential decreases logarithmically with increasing concentration, which is close to Manning-like counterion condensation.[48,49] With regard to PAA-*g*-dodecyl-34%, it is noteworthy that the ζ potential remains unchanged over a concentration range from 0.1 to 0.8 mg ml^{-1}, and it decreases with increasing concentration above 0.9 mg ml^{-1} in addition to the slight decrease below 0.1 mg ml^{-1}. According to the theory of the counterion condensation of hydrophobic polyelectrolytes proposed by Dobrynin and Rubinstein,[20] the condensation of counterions around the chains of hydrophobic polyelectrolytes is relevant to the electrostatic interaction between a hydrophobic bead and a counterion at its surface in the units of thermal energy kT, ε_c, which is expressed as follows:

$$\varepsilon_c \approx \left(\frac{l_B}{bf_i}\right)^{1/3} \tau \quad (3)$$

Here, τ denotes the ratio of reduced temperature, and it is expressed as follows:

$$\tau = (\theta - T)/\theta \quad (4)$$

Clear counterion condensation occurs when ε_c ranges from 0 to 2.5 above a certain concentration. In this study, the ratio of reduced temperature τ ranges from 0 to 1. Meanwhile, according

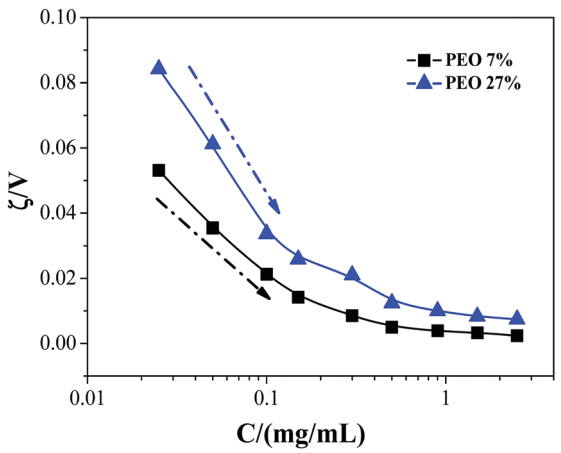

Fig. 8 The concentration dependency of ζ potential for PAA-*g*-PEO molecules in an aqueous solution.

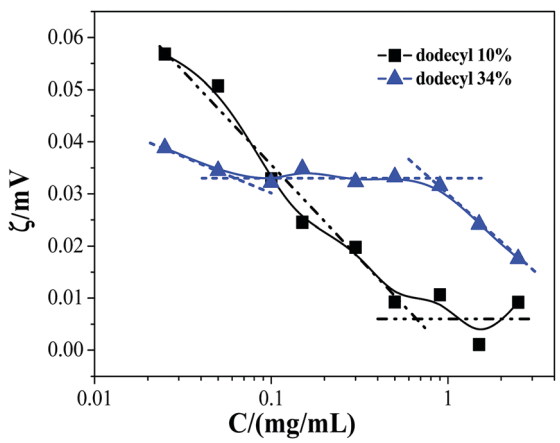

Fig. 9 The concentration dependency of the ζ potential for PAA-*g*-dodecyl molecules in an aqueous solution.

to the method described in a previous study, the fraction of the effective charges of PAA-*g*-dodecyl-34% molecules in solution at 0.025 mg ml^{-1} was estimated to be about 0.187.[36] Then, ε_c was calculated to be in the range of 0–2.5 by substituting Bjerrum length (l_B) of ~0.7 nm, monomer size (b) of ~0.252 nm,[50] and τ into eqn (3). Thus, according to the theory of counterion condensation of hydrophobic polyelectrolytes described above, clear counterion condensation is observed above 0.9 mg ml^{-1} from the blue line in Fig. 9. This phenomenon can be ascribed to the presence of hydrophobic beads that are composed of dodecyl side chains. Above 0.9 mg ml^{-1}, a part of the counterions around these chains spontaneously condenses into hydrophobic beads as the concentration increases. The process of counterion condensation neutralizes some charges on these chains and screens Coulomb repulsion interaction between the monomers to a certain degree. Polyelectrolyte chains further collapse, and the size of hydrophobic beads increases due to the screening of Coulomb repulsion. After that, more counterions start to condense into the hydrophobic beads with a relatively low dielectric constant.[20] The result in Fig. 9 confirms that the behavior of the counterion condensation of PAA-*g*-dodecyl is affected by grafting density. When the grafting density is relatively high, the behavior of counterion condensation mainly occurs above a certain concentration. This is analogous to the behavior of counterion condensation of hydrophobic polyelectrolytes.

4.3 The role of grafting density in chain conformations

In Section 4.1, the critical aggregation concentration (c_p^r) values of PAA-*g*-PEO and PAA-*g*-dodecyl molecules in solution were determined. The results showed that the c_p^r values are influenced by the grafting density. In this section, to determine microscopic information about chain sizes, the values of correlation length (ξ) of PAA-*g*-PEO and PAA-*g*-dodecyl molecules in an aqueous solution (Table 2) were plotted against the concentration (please see Fig. 10).

In addition, we are interested in the effect of grafting density on the degree of intramolecular or intermolecular aggregations. In general, the distribution of counterions around a chain or the linear density of counterions (ρ) is strongly determined by the degree of intramolecular or intermolecular aggregations and the fraction of effective charges.[51,52] By contrast, the ζ potential is only related to the fraction of the effective charges on a chain. In other words, for example, if the ratio of the linear density of the counterions of PAA-*g*-PEO-27% to that of PAA-*g*-PEO-7% is equal to the ratio of the fraction of the effective charges between the two, namely, $\zeta_{\text{PAA-}g\text{-PEO-27\%}}/\zeta_{\text{PAA-}g\text{-PEO-7\%}} = \rho_{\text{PAA-}g\text{-PEO-27\%}}/\rho_{\text{PAA-}g\text{-PEO-7\%}}$, there would be no difference in the density of the intramolecular or intermolecular aggregations between the PAA-*g*-PEO-7% and PAA-*g*-PEO-27% molecules in solution. As another example, if the ratio of the fraction of the effective charges of PAA-*g*-PEO-27% to that of PAA-*g*-PEO-7% is smaller than their ratio of the linear density of the counterions, namely, $\rho_{\text{PAA-}g\text{-PEO-27\%}}/\rho_{\text{PAA-}g\text{-PEO-7\%}} < \zeta_{\text{PAA-}g\text{-PEO-27\%}}/\zeta_{\text{PAA-}g\text{-PEO-7\%}}$, the degree of intramolecular association or intermolecular aggregation of PAA-*g*-PEO-27% molecules is higher. Thus, to compare the degree of intramolecular or intermolecular aggregation between PAA-*g*-PEO-7% and PAA-*g*-PEO-27% or that between PAA-*g*-dodecyl-10% and PAA-*g*-dodecyl-34%, we calculated $\zeta_{\text{PAA-}g\text{-PEO-27\%}}/\zeta_{\text{PAA-}g\text{-PEO-7\%}}$ or $\rho_{\text{PAA-}g\text{-PEO-27\%}}/\rho_{\text{PAA-}g\text{-PEO-7\%}}$ and $\rho_{\text{PAA-}g\text{-dodecyl-34\%}}/\rho_{\text{PAA-}g\text{-dodecyl-10\%}}$ or $\zeta_{\text{PAA-}g\text{-dodecyl-34\%}}/\zeta_{\text{PAA-}g\text{-dodecyl-10\%}}$ by using the values of ζ and ρ shown in Table 2. The results of their concentration dependency are shown in Fig. 11a and b.

Mathematically, according to the DLP theory of flexible polyelectrolytes in solution proposed by Lu *et al.*,[34] the linear density of counterions around chain ρ and zeta potential ζ exhibits the following relationship:

$$\rho \propto \frac{\pi\varepsilon_0\varepsilon_s\zeta}{K_0(\kappa a)} \propto \frac{\zeta}{\kappa^{-1}} \tag{5}$$

As mentioned in Section 2, a is the radius of the stiff charged cylinders on a polyelectrolyte chain composed of many stiff charged cylinders with a radius of a, and κ^{-1} is the thickness of the electric double layer (EDL) around a stiff charged cylinder. $K_0(x)$ is the modified Bessel function of the second kind that can be used to describe the distribution of electric potential around the charged cylinder, where $K_0(\kappa a)$ decreases with an

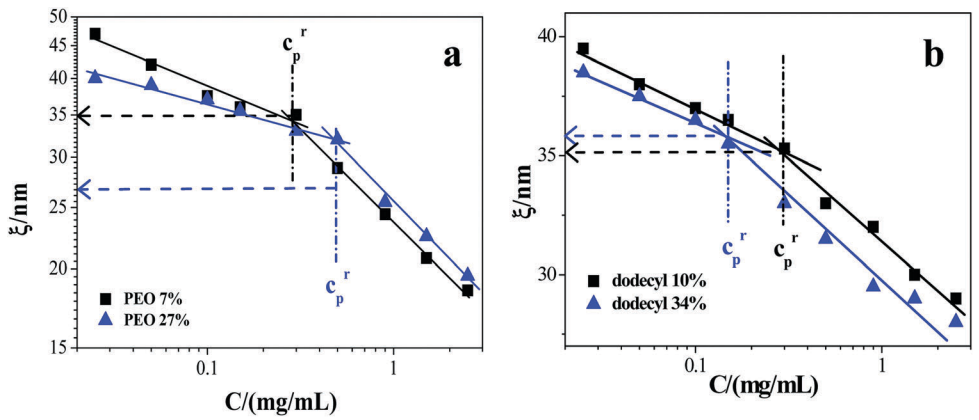

Fig. 10 The concentration dependency of correlation length of (a) PAA-*g*-PEO and (b) PAA-*g*-dodecyl molecules in an aqueous solution. c_p^r represents the critical aggregation concentration.

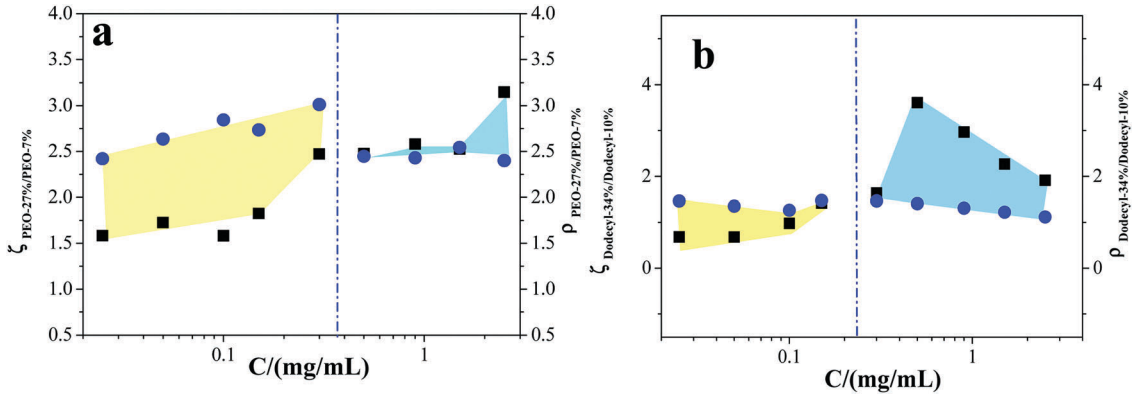

Fig. 11 The ratio of zeta potential and the ratio of linear density of counterions (a) between the PAA-*g*-PEO molecules with two grafting densities and (b) between PAA-*g*-dodecyl molecules with two grafting densities in solution at different concentrations. Blue dash-dot lines represent the position near the critical aggregation concentration c_p^r.

increase in κ.[53] The following equations can be derived from eqn (5):

$$\frac{\kappa_{\text{PAA-}g\text{-PEO-27\%}}{}^{-1}}{\kappa_{\text{PAA-}g\text{-PEO-7\%}}{}^{-1}} \propto \frac{\zeta_{\text{PAA-}g\text{-PEO-27\%}}/\zeta_{\text{PAA-}g\text{-PEO-7\%}}}{\rho_{\text{PAA-}g\text{-PEO-27\%}}/\rho_{\text{PAA-}g\text{-PEO-7\%}}} \quad (6)$$

and

$$\frac{\kappa_{\text{PAA-}g\text{-dodecyl-34\%}}{}^{-1}}{\kappa_{\text{PAA-}g\text{-dodecyl-10\%}}{}^{-1}} \propto \frac{\zeta_{\text{PAA-}g\text{-dodecyl-34\%}}/\zeta_{\text{PAA-}g\text{-dodecyl-10\%}}}{\rho_{\text{PAA-}g\text{-dodecyl-34\%}}/\rho_{\text{PAA-}g\text{-dodecyl-10\%}}} \quad (7)$$

According to eqn (6) and (7), the ratio of $\zeta_{\text{PAA-}g\text{-PEO-27\%}}/\zeta_{\text{PAA-}g\text{-PEO-7\%}}$ to $\rho_{\text{PAA-}g\text{-PEO-27\%}}/\rho_{\text{PAA-}g\text{-PEO-7\%}}$ is proportional to $\kappa_{\text{PAA-}g\text{-PEO-27\%}}{}^{-1}/\kappa_{\text{PAA-}g\text{-PEO-7\%}}{}^{-1}$; meanwhile, the ratio of $\zeta_{\text{PAA-}g\text{-dodecyl-34\%}}/\zeta_{\text{PAA-}g\text{-dodecyl-10\%}}$ to $\rho_{\text{PAA-}g\text{-dodecyl-34\%}}/\rho_{\text{PAA-}g\text{-dodecyl-14\%}}$ is proportional to $\kappa_{\text{PAA-}g\text{-dodecyl-34\%}}{}^{-1}/\kappa_{\text{PAA-}g\text{-dodecyl-10\%}}{}^{-1}$. Thus, the ratio of κ^{-1} can be used to compare the densities of intramolecular or intermolecular aggregation between the molecules with lower and higher grafting densities. By the fitting process described in Section 3.3, κ^{-1} values at different concentrations were obtained, and the values of $\kappa_{\text{PAA-}g\text{-PEO-27\%}}{}^{-1}/\kappa_{\text{PAA-}g\text{-PEO-7\%}}{}^{-1}$ and $\kappa_{\text{PAA-}g\text{-dodecyl-34\%}}{}^{-1}/\kappa_{\text{PAA-}g\text{-dodecyl-10\%}}{}^{-1}$ were calculated. Fig. 12a and b show the concentration dependency of κ^{-1} for PAA-*g*-PEO and PAA-*g*-dodecyl, respectively. Fig. 12c and d show the concentration dependency of $\kappa_{\text{PAA-}g\text{-PEO-27\%}}{}^{-1}/\kappa_{\text{PAA-}g\text{-PEO-7\%}}{}^{-1}$ and $\kappa_{\text{PAA-}g\text{-dodecyl-34\%}}{}^{-1}/\kappa_{\text{PAA-}g\text{-dodecyl-10\%}}{}^{-1}$, respectively. Based on the results obtained from Fig. 9–11 and the above discussion, we will further explore the effect of grafting density on chain conformation in detail.

4.3.1 PAA-*g*-PEO molecules in aqueous solutions. From Section 4.1, we know that c_p^r of PAA-*g*-PEO-27% is higher than that of PAA-*g*-PEO-7%, indicating that intermolecular aggregation for PAA-*g*-PEO-27% occurs at a higher concentration. In general, the c_p^r value of associative polymers is affected by two factors: the intermolecular interaction of electrostatic repulsion and association below c_p^r. The result in Fig. 8 shows that the intermolecular interaction of electrostatic repulsion of PAA-*g*-PEO-27% is higher, which is a possible reason for the higher c_p^r value. As shown in Fig. 10a, $\xi_{\text{PAA-}g\text{-PEO-7\%}}$ and $\xi_{\text{PAA-}g\text{-PEO-27\%}}$ decrease with increasing concentration, and transition points appear at around 0.25 mg ml^{-1} and 0.5 mg ml^{-1}, respectively, which are close to the c_p^r value mentioned above. Relatively speaking, the decrease in ξ with increasing concentration is more rapid above c_p^r. This result can be due to the interaction of electrostatic screening caused by intermolecular aggregation above c_p^r.[14] Besides, as seen from Fig. 10a, below c_p^r, $\xi_{\text{PAA-}g\text{-PEO-27\%}}$ is smaller than $\xi_{\text{PAA-}g\text{-PEO-7\%}}$; above c_p^r, $\xi_{\text{PAA-}g\text{-PEO-27\%}}$ is larger than $\xi_{\text{PAA-}g\text{-PEO-7\%}}$. We know that PAA molecules containing more PEO side chains have stronger associative interactions. Then, considering the results shown in Fig. 8, it can be concluded that the stronger intramolecular association induced by more PEO side chains contributes toward more collapsed conformation for PAA-*g*-PEO-27% molecules below c_p^r; meanwhile, stronger intramolecular electrostatic repulsion partly contributes toward more stretched conformation above c_p^r.

Next, we discuss the role of grafting density of PEO side chains in the degree of intramolecular association and intermolecular aggregation from the results shown in Fig. 11a, 12a and c. As shown in Fig. 11a, below c_p^r, the values of $\rho_{\text{PAA-}g\text{-PEO-27\%}}/\rho_{\text{PAA-}g\text{-PEO-7\%}}$ are higher than those of $\zeta_{\text{PAA-}g\text{-PEO-27\%}}/\zeta_{\text{PAA-}g\text{-PEO-7\%}}$; above c_p^r, the values of $\rho_{\text{PAA-}g\text{-PEO-27\%}}/\rho_{\text{PAA-}g\text{-PEO-7\%}}$ are slightly smaller than those of $\zeta_{\text{PAA-}g\text{-PEO-27\%}}/\zeta_{\text{PAA-}g\text{-PEO-7\%}}$. This indicates that PAA-*g*-PEO-27% has a higher degree of intramolecular association than PAA-*g*-PEO-7% below c_p^r and a slightly lower density of intermolecular aggregation above c_p^r. The higher degree of intramolecular association of PAA-*g*-PEO-27% molecules originates from their more collapsed conformation, which has been proven in Fig. 10a.

From Fig. 12c, it is evident that the value of $\frac{\kappa_{\text{PAA-}g\text{-PEO-27\%}}{}^{-1}}{\kappa_{\text{PAA-}g\text{-PEO-7\%}}{}^{-1}}$ is smaller than 1 below c_p^r and larger than 1 above c_p^r. According to eqn (6), the value of $\zeta_{\text{PAA-}g\text{-PEO-27\%}}/\zeta_{\text{PAA-}g\text{-PEO-7\%}}$ is smaller than the value of $\rho_{\text{PAA-}g\text{-PEO-27\%}}/\rho_{\text{PAA-}g\text{-PEO-7\%}}$ below c_p^r, and the former is larger than the latter above c_p^r. This result also suggests that PAA-*g*-PEO-27% molecules collapse more than PAA-*g*-PEO-7% molecules below c_p^r, and the density of intermolecular aggregation of PAA-*g*-PEO-27% is lower than that of PAA-*g*-PEO-7% above c_p^r.

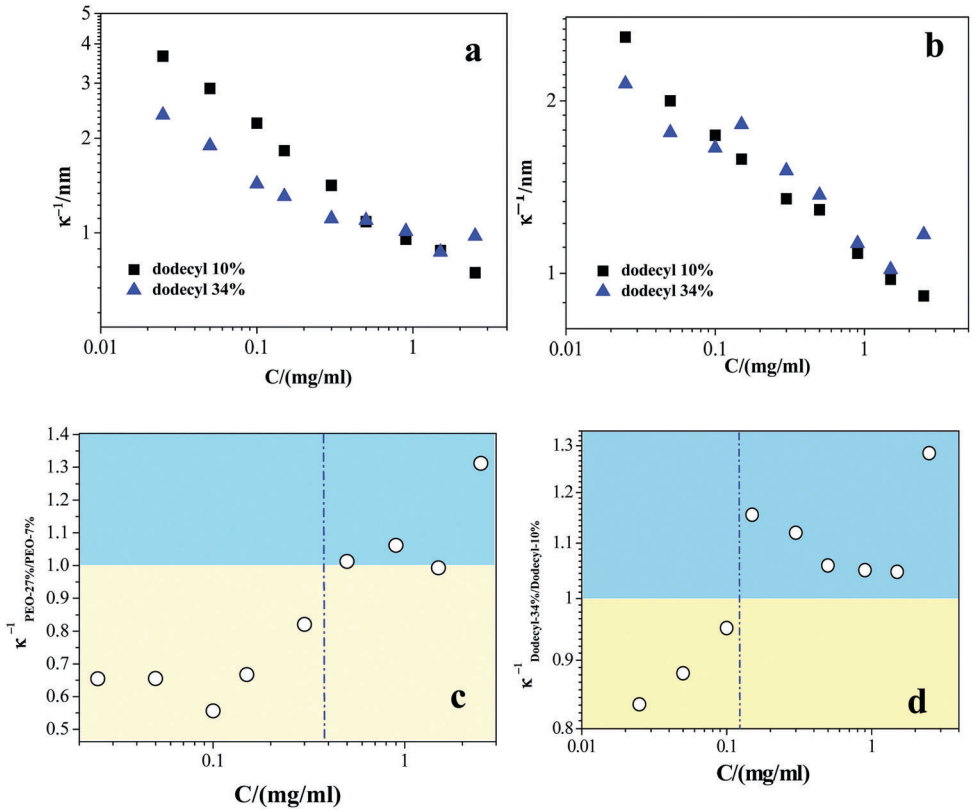

Fig. 12 The concentration dependency of Debye lengths of (a) PAA-*g*-PEO molecules and (b) PAA-*g*-dodecyl molecules in solution and the ratio of Debye lengths (c) between molecules with two grafting densities in solution for (c) PAA-*g*-PEO and for (d) PAA-*g*-dodecyl. In the blue regions, the value of the ratio of Debye length is larger than 1; in the yellow regions, it is smaller than 1. The blue dash-dot lines represent the position near the critical aggregation concentration c_p^r.

Moreover, we make another attempt to compare the densities of intermolecular aggregations between PAA-*g*-PEO-27% and PAA-*g*-PEO-7% molecules above c_p^r by analyzing the results of ζ in Fig. 8 and κ^{-1} in Fig. 12a. As shown in Fig. 8, above c_p^r, $\zeta_{\text{PAA-}g\text{-PEO-27\%}}$ was larger than $\zeta_{\text{PAA-}g\text{-PEO-7\%}}$. This indicated that the concentration of counterions in the solution of PAA-*g*-PEO-27% ($q_{\text{c-PAA-}g\text{-PEO-27\%}}$) was higher than that in the solution of PAA-*g*-PEO-7% ($q_{\text{c-PAA-}g\text{-PEO-7\%}}$). According to eqn (2), ${\kappa_{\text{PAA-}g\text{-PEO-27\%}}}^{-1}$ should have been smaller than ${\kappa_{\text{PAA-}g\text{-PEO-7\%}}}^{-1}$. However, as shown in Fig. 12a, ${\kappa_{\text{PAA-}g\text{-PEO-27\%}}}^{-1}$ was larger than ${\kappa_{\text{PAA-}g\text{-PEO-7\%}}}^{-1}$ above c_p^r. It is predictable that if the density of intermolecular aggregation is lower, the density of counterions around a chain will be lower, because of which the electrostatic interaction between the monomers on the chain is neutralized in a longer scale of κ^{-1}. This point has been stated in some studies.[54,55] Thus, the larger ${\kappa_{\text{PAA-}g\text{-PEO-27\%}}}^{-1}$ value implied that the density of intermolecular aggregation of PAA-*g*-PEO-27% in an aqueous solution was lower than that of PAA-*g*-PEO-7%.

In short, we can generally conclude that PAA molecules grafting more PEO side chains are more susceptible to collapse below c_p^r and exhibit intermolecular aggregation with a lower density above c_p^r. From Fig. 8, it is confirmed that intramolecular and intermolecular electrostatic interactions of PAA-*g*-PEO-27% molecules are stronger than those of PAA-*g*-PEO-7% molecules. Thus, one of the most possible reasons for the more collapsed conformation of PAA-*g*-PEO-27% molecules below c_p^r is the stronger intramolecular association introduced by more PEO side chains. Meanwhile, stronger intermolecular association with electrostatic repulsive interactions may lead to intermolecular aggregation with a lower density above c_p^r.

4.3.2 PAA-*g*-dodecyl molecules in aqueous solutions. From Section 4.1.2, it was inferred that the critical aggregation concentration (c_p^r) value of PAA-*g*-dodecyl-34% was lower than that of PAA-*g*-dodecyl-34%. This indicated that the intermolecular aggregation for PAA-*g*-PEO-27% occurred at a lower concentration. From Fig. 9, we know that the interaction of intermolecular electrostatic repulsion for PAA-*g*-PEO-27% is weaker below c_p^r. Therefore, the lower c_p^r value might be the result of stronger intermolecular associative interactions caused by more dodecyl side chains. As shown in Fig. 10b, $\xi_{\text{PAA-}g\text{-dodecyl-34\%}}$ is smaller than $\xi_{\text{PAA-}g\text{-dodecyl-10\%}}$ over the total concentration range, suggesting that PAA-*g*-dodecyl-34% molecules were more collapsed than PAA-*g*-dodecyl-10% molecules. Here, the chain conformation of PAA-*g*-dodecyl molecules in solution was the result of the delicate balance of interactions of electrostatic repulsion between the monomers and intramolecular hydrophobic associations between the dodecyl side chains.[56] Fig. 9 shows that the electrostatic interaction between the monomers of PAA-*g*-dodecyl-34% is weaker below c_p^r; inversely, it is stronger above c_p^r. Therefore, below c_p^r, the weaker interaction

of electrostatic repulsion and stronger hydrophobic association interaction for PAA-*g*-dodecyl-34% contribute toward more collapsed conformations; above c_p^r, the stronger interaction of intramolecular hydrophobic association mainly contributes toward more collapsed conformation.

Similar to that in Section 4.3.1, we now discuss the role of grafting density of dodecyl side chains in the degree of intramolecular association and intermolecular aggregation on the basis of the results in Fig. 11b, 12b and d. As shown in Fig. 11b, below c_p^r, $\rho_{PAA\text{-}g\text{-}dodecyl\text{-}34\%}/\rho_{PAA\text{-}g\text{-}dodecyl\text{-}10\%}$ is larger than $\zeta_{PAA\text{-}g\text{-}dodecyl\text{-}34\%}/\zeta_{PAA\text{-}g\text{-}dodecyl\text{-}10\%}$. By contrast, above c_p^r, $\rho_{PAA\text{-}g\text{-}dodecyl\text{-}34\%}/\rho_{PAA\text{-}g\text{-}dodecyl\text{-}10\%}$ is remarkably lower than $\zeta_{PAA\text{-}g\text{-}dodecyl\text{-}34\%}/\zeta_{PAA\text{-}g\text{-}dodecyl\text{-}10\%}$. This indicates that PAA-*g*-dodecyl-34% molecules are more collapsed than PAA-*g*-dodecyl-10% below c_p^r, and the density of intermolecular aggregation of PAA-*g*-dodecyl-34% is smaller than that of PAA-*g*-dodecyl-10% above c_p^r. Moreover, from Fig. 12d, below c_p^r, it can be observed that the values of $\kappa_{PAA\text{-}g\text{-}dodecyl\text{-}34\}^{-1}/\kappa_{PAA\text{-}g\text{-}dodecyl\text{-}10\}^{-1}$ are smaller than 1; above c_p^r, the values of $\kappa_{PAA\text{-}g\text{-}dodecyl\text{-}34\}^{-1}/\kappa_{PAA\text{-}g\text{-}dodecyl\text{-}10\}^{-1}$ are larger than 1. According to eqn (7), we know that the values of $\rho_{PAA\text{-}g\text{-}dodecyl\text{-}34\%}/\rho_{PAA\text{-}g\text{-}dodecyl\text{-}10\%}$ are higher than those of $\zeta_{PAA\text{-}g\text{-}dodecyl\text{-}34\%}/\zeta_{PAA\text{-}g\text{-}dodecyl\text{-}10\%}$. The values of $\rho_{PAA\text{-}g\text{-}dodecyl\text{-}34\%}/\rho_{PAA\text{-}g\text{-}dodecyl\text{-}10\%}$ are remarkably lower than those of $\zeta_{PAA\text{-}g\text{-}dodecyl\text{-}34\%}/\zeta_{PAA\text{-}g\text{-}dodecyl\text{-}10\%}$, which is consistent with the results shown in Fig. 11b.

Moreover, as shown in Fig. 9, above c_p^r, $\zeta_{PAA\text{-}g\text{-}dodecyl\text{-}34\%}$ is larger than $\zeta_{PAA\text{-}g\text{-}dodecyl\text{-}10\%}$, indicating that the concentration of the counterions of PAA-*g*-dodecyl-34% molecules in solution is higher than that of PAA-*g*-dodecyl-10% molecules, *i.e.*, $q_{c\text{-}PAA\text{-}g\text{-}dodecyl\text{-}34\%} > q_{c\text{-}PAA\text{-}g\text{-}dodecyl\text{-}10\%}$. According to eqn (2), $\kappa_{PAA\text{-}g\text{-}dodecyl\text{-}34\}^{-1}$ should have been smaller than $\kappa_{PAA\text{-}g\text{-}dodecyl\text{-}10\}^{-1}$. However, from Fig. 12b, we found that the value of $\kappa_{PAA\text{-}g\text{-}dodecyl\text{-}34\}^{-1}$ was larger than that of $\kappa_{PAA\text{-}g\text{-}dodecyl\text{-}10\}^{-1}$. This also implies that the density of intermolecular aggregation of PAA-*g*-dodecyl-34% is lower than that of PAA-*g*-dodecyl-10% above c_p^r.

In short, we can generally conclude that PAA molecules grafting more dodecyl side chains form intermolecular aggregation with lower density above c_p^r. From Fig. 9, it is confirmed that the intramolecular and intermolecular electrostatic interactions of PAA-*g*-dodecyl-34% molecules are weaker than those of PAA-*g*-dodecyl-10% molecules below c_p^r, and they are stronger than those of PAA-*g*-dodecyl-10% molecules above c_p^r. Thus, intermolecular aggregations with lower densities may be the result of stronger interactions with intermolecular electrostatic repulsion.

5. Conclusion

The dielectric behaviors of PAA-*g*-PEO-7%, PAA-*g*-PEO-27%, PAA-*g*-dodecyl-10%, and PAA-*g*-dodecyl-34% molecules in aqueous solutions were measured from 40 Hz to 110 MHz over a concentration range from 0.025 mg ml^{-1} to 2.5 mg ml^{-1}. Two relaxations were observed after eliminating electrode polarization. By analyzing the dielectric spectra with the DLP model of flexible polyelectrolytes, many valuable internal structural and electrical parameters were obtained.

The results of ζ potential indicate that grafting more PEO side chains promotes the ionization of polyelectrolytes, and grafting more dodecyl side chains leads to strong counterion condensation above a certain concentration. The critical aggregation concentrations were determined by the concentration dependency of dielectric parameters. Considering electric charge characteristics of molecules, we clarified the effect of grafting density on chain conformation. For PAA-*g*-PEO-27% molecules, below the critical aggregation concentration, more PEO side chains induced stronger intramolecular H-bond association interactions; thus, the molecules adopted a more collapsed conformation. Above the critical aggregation concentration, more PEO side chains induced stronger intermolecular electrostatic repulsion; therefore, the degree of intermolecular association was lower. For PAA-*g*-dodecyl-34% molecules, below the critical aggregation concentration, more dodecyl side chains induced stronger intramolecular hydrophobic association interaction and lower electrostatic repulsion between the monomers; thus, the molecules adopted a more collapsed conformation. Above the critical aggregation concentration, more dodecyl side chains induced higher intermolecular electrostatic repulsion; therefore, the degree of intermolecular association was lower.

This study not only facilitates a better understanding of chain conformations of polyelectrolytes containing side chains in solution, but also proves that dielectric analysis based on the double-layer polarization model can be a promising tool to investigate chain conformations of polyelectrolytes.

Conflicts of interest

There are no conflicts to declare.

Acknowledgements

The authors gratefully thank Dr Jin-kun Hao, from the Institute of Chemistry, the Chinese Academy of Science, for kindly providing the samples used in this study. Financial support for this work from the National Natural Science Foundation of China (No. 21673002, 21473012 and 21173025) is gratefully acknowledged.

References

1 P. Alexandridis, J. F. Holzwarth and T. A. Hatton, Micellization of poly(ethylene oxide)–poly(propylene oxide)–poly(ethylene oxide) triblock copolymer in aqueous solutions: thermodynamics of copolymer association, *Macromolecules*, 1994, **27**, 2414–2425.

2 M. Suwa, A. Hashidzume, Y. Morishima, T. Nakato and M. Tomida, Self-association behavior of hydrophobically modified poly(aspartic acid) in water studied by fluorescence and dynamic light scattering techniques, *Macromolecules*, 2000, **33**, 7884–7892.

3 W. Y. Liu, Y. J. Liu, G. S. Zeng, R. G. Liu and Y. Huang, Coil-to-rod conformational transition and single chain

structure of graft copolymer by tuning the graft density, *Polymer*, 2012, **53**, 1005–1014.
4 H. Morinaga, H. Morikaw, Y. Wang, A. Sudo and T. Endo, Amphiphilic copolymer having acid-labile acetal in the side chain as a hydrophobe: controlled release of aldehyde by thermoresponsive aggregation–dissociation of polymer micelles, *Macromolecules*, 2009, **42**, 2229–2235.
5 C. L. Gebhart and A. V. Kabanov, Perspectives on polymeric gene delivery, *J. Bioact. Compat. Polym.*, 2003, **18**, 147–166.
6 D. Schmaljohann, Thermo-and pH-responsive polymers in drug delivery, *Adv. Drug Delivery Rev.*, 2006, **58**, 1655–1970.
7 M. Yokoyama, Gene delivery using temperature-responsive polymeric carriers, *Drug Discovery Today*, 2002, **7**, 426–432.
8 K. Kataoka, A. Harada and Y. Nagasaki, Block copolymer micelles for drug delivery: design, characterization and biological significance, *Adv. Drug Delivery Rev.*, 2001, **47**(1), 113–131.
9 A. Kikuchi and T. Nose, Unimolecular-micelle formation of poly(methyl methacrylate)-*graft*-polystyrene in iso-amyl acetate, *Polymer*, 1996, **37**, 5889–5896.
10 S. Halacheva, G. J. Price and V. M. Garamus, Effects of temperature and polymer composition upon the aqueous solution properties of comblike linear poly(ethylene imine)/poly(2-ethyl-2-oxazoline)-based polymers, *Macromolecules*, 2011, **44**, 7394–7404.
11 O. V. Borisov and E. B. Zhulina, Amphiphilic graft copolymer in a selective solvent: intramolecular structures and conformational transitions, *Macromolecules*, 2005, **38**, 2506–2514.
12 Y. Rouault and O. V. Borisov, Comb-branched polymers: Monte Carlo simulation and scaling, *Macromolecules*, 1996, **29**, 2605–2611.
13 J. L. Li and K. S. Zhao, Effect of side-chain on conformation of poly(acrylic acid) and its dielectric behaviors in aqueous solution: hydrophobic and hydrogen-bonding interactions and mechanism of relaxations, *J. Phys. Chem. B*, 2013, **117**, 11843–11852.
14 J. K. Hao, Z. Y. Li, H. Cheng, C. Wu and C. C. Han, Kinetically driven intra- and interchain association of hydrophobically and hydrophilically modified poly(acrylic acid) in dilute aqueous solutions, *Macromolecules*, 2010, **43**, 9534–9540.
15 D. P. Garrett, L. J. William, W. S. Charles and L. M. Charles, Enhanced coil expansion and intrapolymer complex formation of linear poly(methacrylic acid) containing poly(ethylene glycol) grafts, *Macromolecules*, 2004, **37**, 2603–2612.
16 K. Chandrasekar and G. Baskar, Investigations of the dissociation behavior and interfacial adsorption characteristics of polyelectrolytes from poly(acryamido-2-methyl-1-propane sulfonic acid) with an octadecyl side chain, *J. Polym. Sci., Part A: Polym. Chem.*, 2006, **44**, 314–324.
17 K. Benmansour, A. Mansri and J. Francois, Oligo(ethylene oxide) side-chain steric screening effects on conductimetric properties of grafted poly(4-vinylpyridinium) salts in aqueous solutions, *Polym. Int.*, 2003, **52**, 1506–1514.
18 J. Weber, V. Boyko and K. F. Arndt, Influence of grafting on the solution properties and the dissociation behavior of ionic/nonionic grafted copolymers, *Macromol. Chem. Phys.*, 2007, **208**, 643–650.
19 W. Essafi, F. Lafuma and C. E. Williams, Anomalous counterion condensation in salt-free hydrophobic polyelectrolyte solutions: osmotic pressure measurements, *Europhys. Lett.*, 2005, **71**(6), 938–944.
20 A. V. Dobrynin and M. Rubinstein, Counterion condensation and phase separation in solutions of hydrophobic polyelectrolytes, *Macromolecules*, 2001, **34**, 1964–1972.
21 C. Wandrey, D. Hunkeler, U. Wendler and W. Jaeger, Counterion activity of highly charged polyelectrolytes, *Macromolecules*, 2000, **33**, 7136–7143.
22 T. Miyajima and M. M. Ishguro, Analysis of complexation equilibria of polyacrylic acid by a donnan-based concept, *J. Colloid Interface Sci.*, 1997, **187**, 259–266.
23 I. Pochard, A. Foissy and P. Couchot, Conductometric and microcalorimetric analysis of the alkaline-earth/alkali-metal ion exchange onto polyacrylic acid, *J. Colloid Interface Sci.*, 1999, **277**, 818–827.
24 J. Blaul, M. Wittemann, M. Ballauff and M. Rehahn, Osmotic coefficient of a synthetic rodlike polyelectrolyte in salt-free solution as a test of the Poisson-Boltzmann cell model, *J. Phys. Chem. B*, 2000, **104**, 7077–7081.
25 D. Hinderberger, H. W. Spiess and G. Jeschke, Separation of polyelectrolyte chain dynamics and dynamics of counterion attachment by EPR spectroscopy, *Macromol. Symp.*, 2004, **211**, 71–86.
26 D. Hinderberger, H. W. Spiess and G. Jeschke, Radial counterion distributions in polyelectrolyte solutions determined by EPR spectroscopy, *Europhys. Lett.*, 2005, **70**, 102–108.
27 Z. Chen, X. W. Li, K. S. Zhao, J. X. Xiao and L. K. Yang, Dielectric spectroscopy investigation on the interaction of poly(diallyldimethylammonium chloride) with sodium decyl sulfate in aqueous solution, *J. Phys. Chem. B*, 2011, **115**(19), 5766–5774.
28 D. Truzzolillo, C. Cametti and S. Sennatoab, Dielectric properties of differently flexible polyions: a scaling approach, *Phys. Chem. Chem. Phys.*, 2009, **11**, 1780–1786.
29 M. Luksic, R. Buchner, B. Hribar-Lee and V. Vlachy, Dielectric relaxation spectroscopy of aliphatic ionene bromides and fluorides in water: the role of the polyion' s charge density and the nature of the counterions, *Macromolecules*, 2009, **42**(12), 4337–4342.
30 T. Mitsumata, T. Miura, N. Takahashi, M. Kawai, M. K. Okajima and T. Kaneko, Ionic state and chain conformation for aqueous solutions of supergiant cyanobacterial polysaccharide, *Phys. Rev. E*, 2013, **87**, 042607.
31 F. van der Touw and M. Mandel, Dielectric increment and dielectric dispersion of solutions containing simple charged linear macromolecules: I. Theory, *Biophys. Chem.*, 1974, **2**, 218–230.
32 K. Ito, A. Yagi, N. Ookubo and R. Hayakawa, Crossover behavior in high-frequency dielectric relaxation of linear polyions in dilute and semidilute solutions, *Macromolecules*, 1990, **23**, 857–862.

33 M. Fixman, Charged macromolecules in external fields. I. The sphere, *J. Chem. Phys.*, 1980, **72**, 5177–5186.
34 C. Y. David, Lu, Theory of the polyelectrolyte dielectric function, *Phys. Rev. E*, 2011, **84**, 041804.
35 X. L. Zhou and K. S. Zhao, How side chains affect conformation and electrical properties of poly(acrylic acid) in solution?, *Phys. Chem. Chem. Phys.*, 2017, **19**, 20559–20572.
36 X. L. Zhou and K. S. Zhao, Chain conformation of poly(acrylic acid)-*graft*-poly(ethylene oxide)-*graft*-dodecyl in solution: an anomalous counterions condensation, *Soft Matter*, 2018, **14**, 1130–1141.
37 H. Schwan, Determination of biological impedances, in *Physical Techniques in Biological Research*, ed. W. L. Nastuk, Academic Press, Inc., New York, 1963.
38 H. S. Harned and R. L. Nuttall, The differential diffusion coefficient of potassium chloride in aqueous solutions, *J. Am. Chem. Soc.*, 1949, **71**, 1460–1463.
39 K. Asami, Characterization of heterogeneous systems by dielectric spectroscopy, *Prog. Polym. Sci.*, 2002, **27**, 1617–1659.
40 A. V. Dobrynin and M. Rubinstein, Theory of polyelectrolytes in solutions and at surfaces, *Prog. Polym. Sci.*, 2005, **30**, 1049–1118.
41 J. L. Li, K. S. Zhao and C. Y. Liu, Dielectric relaxations of poly(acrylic acid)-*graft*-poly(ethylene oxide) aqueous solution: analysis coupled with scaling approach and hydrogen-bonding complex, *Phys. Rev. E: Stat., Nonlinear, Soft Matter Phys.*, 2013, **87**, 042603.
42 B. H. Zimm, Dynamics of polymer molecules in dilute solution: viscoelasticity, flow birefringence and dielectric loss, *J. Chem. Phys.*, 1956, **24**, 269–278.
43 I. Tomatsu, A. Hashidzume and A. Harada, Gel-to-sol and sol-to-gel transitions utilizing the interaction of a-cyclodextrin with dodecyl side chains attached to a poly(acrylic acid) backbone, *Macromol. Rapid Commun.*, 2005, **26**, 825–829.
44 B. Magny, I. Iliopoulos and R. Audebert, Intrinsic viscosity of hydrophobically modified polyelectrolytes, *Polym. Commun.*, 1991, **32**, 456–458.
45 C. Senan, J. Meadows, P. T. Shone and P. A. Williams, Solution behavior of hydrophobically modified sodium polyacrylate, *Langmuir*, 1994, **10**, 2471–2479.
46 F. Petit, I. Iliopoulos, R. Audebert and S. Szönyi, Associating polyelectrolytes with perfluoroalkyl side chains: aggregation in aqueous solution, association with surfactants, and comparison with hydrogenated analogues, *Langmuir*, 1997, **13**, 4229–4233.
47 K. J. Tielrooij, J. Hunger, R. Buchner, M. Bonn and H. J. Bakker, Influence of Concentration and Temperature on the Dynamics of Water in the Hydrophobic Hydration Shell of Tetramethylurea, *J. Am. Chem. Soc.*, 2010, **132**, 15671–15678.
48 G. S. Manning, A condensed counterion theory for polarization of polyelectrolyte solutions in high fields, *J. Chem. Phys.*, 1993, **99**, 477–486.
49 G. S. Manning, Limiting laws and counterion condensation in polyelectrolyte solutions I. Colligative properties, *J. Chem. Phys.*, 1969, **51**, 924–933.
50 Y. Mylonas, G. Staikos and M. Ullner, Chain conformation and intermolecular interaction of partially neutralized poly(acrylic acid) in dilute aqueous solutions, *Polymer*, 1999, **40**, 6841–6847.
51 S. Liu and M. Muthukumar, Langevin dynamics simulation of counterion distribution around isolated flexible polyelectrolyte chains, *J. Chem. Phys.*, 2002, **116**, 9975–9982.
52 A. Chremos and J. F. Douglas, Counter-ion distribution around flexible polyelectrolytes having different molecular architecture, *Soft Matter*, 2016, **12**, 2932–2941.
53 G. Källen, *Quantum Electrodynamics*, Springer, Berlin, 1972.
54 M. Muthukumar, 50th Anniversary Perspective: A Perspective on Polyelectrolyte Solutions, *Macromolecules*, 2017, **50**, 9528–9560.
55 A. R. Denton, Counterion penetration and effective electrostatic interactions in solutions of polyelectrolyte stars and microgels, *Phys. Rev. E*, 2003, **67**, 011804.
56 K. T. Wang, I. Liopoulos and R. Audebert, Viscometric behaviour of hydrophobically modified poly(sodium acrylate), *Polym. Bull.*, 1988, **20**(6), 577–582.